Design of a Novel Molecular-Imprinted Rh−Amine Complex on SiO_2 and Its Shape-Selective Catalysis for α-Methylstyrene Hydrogenation

Mizuki Tada, Takehiko Sasaki, and Yasuhiro Iwasawa*

Department of Chemistry, Graduate School of Science, The University of Tokyo, Hongo, Bunkyo-ku, Tokyo, 113-0033, Japan

Received: August 13, 2003; In Final Form: October 30, 2003

A new molecular-imprinted Rh−amine complex with a template-shaped cavity acting as a shape-selective reaction space was prepared by metal-complex attaching and molecular imprinting techniques on a SiO_2 surface. $Rh(\eta^3\text{-}C_3H_5)_3$ reacted with SiO_2, and the precursor was attached on the surface to form a bidentate structure $Rh(C_3H_5)(OSi)_2$. α-Methylbenzylamine with a shape similar to that of a half-hydrogenated alkyl intermediate of α-methylstyrene coordinated to the attached Rh as a template ligand. Then SiO_2−matrix overlayers were stacked on the surface by the hydrolysis−polymerization of $Si(OCH_3)_4$ surrounding the attached Rh complexes with the amine template. Final evacuation at 373 K promoted the removal of the template ligand from the Rh complex embedded in the surface pore of the SiO_2−matrix overlayers. All the structures of the attached Rh complexes were characterized by the means of ICP, XPS, ESR, FT-IR, solid-state MAS NMR, EXAFS, DFT, GC, and H_2 adsorption. The imprinted Rh complex has an unsaturated structure Rh(amine)(OSi)(HOSi) and exhibits high catalytic activity for α-methylstyrene hydrogenation. On the contrary, the other supported Rh complexes before imprinting are inactive for the hydrogenation. Furthermore, the active Rh complex is durable under the reaction condition despite the unsaturated conformation which usually tends to gather each other. The imprinted cavity locating on the active Rh center acts as a shape-selective reaction space for α-methylstyrene. The inhibition of the hydrogenation by the use of seven amines with different shapes demonstrates the shape-selective behavior of the imprinted Rh complex discriminating one methyl group and the position of the phenyl ring.

1. Introduction

The functional capability of metals possessing various kinds of forms highly depends on the conformation and environment of the metal species, and the fine construction of metal architecture is key to regulating their property and reactivity. Catalysis is one of the important aspects of the properties of metals,[1−3] and the design of catalytically active structures has been an indispensable issue in the fulfillment of increasing activity, durability, and selectivity. However, the three essential factors of catalysts are often in a tradeoff relationship with each other. The construction of catalytic systems fulfilling these conflicting requirements is difficult based on conventional ideas of catalyst design, and the establishment of new methods and concepts is critical to breaking the present roadblock.

The interaction between active metal species and a support surface creates unique unsaturated active metal structures and protects the aggregation of the metals that is one of the main reasons for deactivation. The delicate design of the location, structure, coordination sphere, and interaction with a support of surface metal species is essential to control the reactivity of the metal sites. Such elaborated surface species are much different from species in bulk or a solution, and the resultant distinct reactivity and phenomena are observed through the unique structure on the surface. However, the characterization of surface species is quite complicated, and it is difficult to understand the key issues relevant to the new design of active sites.[1−3] Further, the regulation of shape selectivity on a surface catalytic species has been especially underdeveloped compared to homogeneous systems, and there are no established methods to prepare shape-selective reaction sites on surfaces. It is vital to find a way to create a catalytically active site on a surface with shape selectivity for a target molecule as to the desired product and reaction.

Very recently, we have proposed a new concept and method for the design of shape-selective reaction spaces on a surface for the first time,[4,5] namely, the molecular imprinting of surface-attached metal complexes, which can provide novel metal species with activity, durability, and selectivity at the same time.[6−9] A Rh complex coordinated with a template phosphite with a shape similar to that of a desired molecule is attached on a SiO_2 surface. Surface SiO_2−matrix overlayers are stacked on the surface surrounding the attached metal complex, and then the template ligand is eliminated from the Rh complex in each pore of the surface−matrix overlayers.[6,7] The unsaturated Rh complexes after the removal of the template phosphite are highly active, and the surface pores prevent the active Rh complexes from decomposing. Further, a template-shaped cavity acting as a shape-selective reaction space is created on the Rh site behind the template ligand.[8]

Molecular imprinting is a method to prepare a space mimicking a template molecule[4,10−14] and is applied to many processes,[15−23] but it is quite difficult to attempt to produce a shape-selective reaction space and to regulate a sequence of dynamic reaction processes beyond simple adsorption. Molecular imprinting has also been applied to bulk materials, where the location of imprinted sites is often heterogeneous and dis-

* Corresponding author. Tel: 81-3-5841-4363. Fax: 81-3-5800-6892. E-mail: iwasawa@chem.s.u-tokyo.ac.jp.

10.1021/jp036421v CCC: $27.50
Published on Web 02/07/2004

advantageous for catalysis. We avoided such problems by using a metal complex attached on a surface, and succeeded in creating remarkable catalysis.[6−8]

In this study, we have prepared a new imprinted Rh−amine complex on a SiO_2 surface by combining the two methods: metal-complex attaching on a SiO_2 surface and molecular imprinting on the surface. Step-by-step reactions to control both coordination and elimination of a template are vital for the design of an imprinted metal complex. Amine is one of the valuable ligands whose reactions can be steadily controlled by the fine adjustment of their reaction conditions. Thus, we chose an amine ligand as a template for the imprinting of an attached Rh complex and designed a sequence of regulated preparation steps for an imprinted metal species on a SiO_2 surface. Furthermore, there are many stable amine ligands with various shapes commercially available. Amine-imprinted complexes make it possible to prepare shape-selective spaces with various shapes on metal sites in the similar imprinting procedure, and it is a quite important point in the preparation of new useful materials.

We also report the characterization and shape-selective hydrogenation activity of the Rh-monomer complex catalyst imprinted with α-methylbenzylamine at a SiO_2 surface. The imprinted Rh complex is highly active for α-methylstyrene hydrogenation, whereas other supported Rh structures before the imprinting have no activity for the reaction. The shape-selective behavior is also observed on the imprinted Rh complex. The strategy is a promising way to design shape-selective reaction sites for any other desired product molecules.

2. Experimental

All procedures were manipulated under nitrogen atmosphere (99.999% purity). All solvents (dehydrated) were purchased from WAKO Chemicals and used without further purification. Rhodium chloride (Aldrich) and a tetrahydrofuran solution of allylmagnesium chloride (Tokyo Kasei Kogyo) were used for the synthesis of a $Rh(\eta^3\text{-}C_3H_5)_3$ precursor. The template L-(−)-α-methylbenzylamine, tetramethoxysilane, and α-methylstyrene were purchased from ACROS Organic, Shinetsu Co., and WAKO Chemicals, respectively. Seven amines used as inhibitors for the catalytic hydrogenation—benzylamine (Tokyo Kasei Kogyo), the template L-(−)-α-methylbenzylamine, (S)-(−)-α,4-dimethylbenzylamine (ACROS Organic), 1-methylheptylamine (Aldrich), (S)-(+)-1-methyl-3-phenylpropylamine (ACROS Organic), benzhydrylamine (Tokyo Kasei Kogyo), and (S)-(−)-1-(1-naphthyl)ethylamine (ACROS Organic) were also stored and handled under nitrogen atmosphere.

Attachment of $Rh(\eta^3\text{-}C_3H_5)_3$. $Rh(\eta^3\text{-}C_3H_5)_3$ was prepared according to the literature.[24] Aerosil 200 (surface area: 200 $m^2\ g^{-1}$) preevacuated at 773 K for 2 h was impregnated with a toluene solution of $Rh(\eta^3\text{-}C_3H_5)_3$ at 295 K. After stirring for 1 h, the solvent was evaporated at room temperature (RT). The obtained yellow sample denoted as $Rh(C_3H_5)/SiO_2$ was stored under N_2. Rh loadings were regulated in the range of 0.2−0.6 wt %.

Coordination of α-Methylbenzylamine (template). The ethanol solution of the template α-methylbenzylamine (2 equiv. to the attached Rh) was added to $Rh(C_3H_5)/SiO_2$ at RT. The color of $Rh(C_3H_5)/SiO_2$ disappeared immediately. After stirring for 30 min, the solvent was evaporated under vacuum. The obtained pale-yellow powder was stored under N_2, which is denoted as Rh_{sup}.

Molecular Imprinting for the Rh_{sup} Complex. Both $Si(OCH_3)_4$ (2.7 g per 1 g of Aerosil 200) and distilled H_2O (1.2 g) were deposited on the surface of Rh_{sup} in a closed batch reactor by chemical vapor deposition (CVD) technique vaporized at 373 K to form SiO_2−matrix overlayers on the Aerosil support. After the deposition at RT, the reactor was heated at 333 K for 7 h, followed by evacuation at the same temperature for 10 h. The obtained complex is denoted as Rh_{imp-b}. To extract the template amine ligand, the Rh_{imp-b} sample was evacuated at 373 K. The complex after the evacuation is denoted as Rh_{imp-a}.

The amount of the SiO_2−matrix overlayers was determined by the weight of the sample evacuated at several high temperatures. The catalyst weight increased by the deposited SiO_2−matrix overlayers and physically adsorbed molecules (water, methanol, etc.). To estimate the contribution of adsorbed molecules to the weight increase, the imprinted material (Rh_{imp-b}) was calcined at 333, 373, 473, 573, 673, and 773 K. The ratio of hydrolyzed $Si(OCH_3)_4$ was estimated from extrapolation to the weight calcined at 773 K.

Analysis of the Amounts of Propene and Propane. The quantitative analyses of propene and propane were carried out for the first and second preparation steps. During each evaporation of the solvent under vacuum, all products were trapped by liquid nitrogen, and the trapped mixture was analyzed by gas chromatography (GC). Three steps were analyzed in the way: the attachment step in a toluene solution for $Rh(C_3H_5)/SiO_2$, the next coordination of the template amine in an ethanol solution, and the coordination of the amine in a toluene solution to compare the effect of solvents. Further, $Rh(C_3H_5)/SiO_2$ and Rh_{sup} complex were treated with hydrogen of 30 kPa in a closed batch reactor in order to estimate the remaining C_3H_5 ligands on the both samples. The gas phases after cooling to RT were also analyzed by GC.

Adsorption of H_2 and CO. The adsorption of H_2 and CO was conducted in a closed batch reactor. Each sample (250 mg) of $Rh(C_3H_5)/SiO_2$, Rh_{sup} complex, and Rh_{imp-a} complex was evacuated at RT for 1 h before the measurement. A dead volume was estimated by helium gas. The adsorption of H_2 was performed at RT in the pressure range 0−101.3 kPa. In addition to the measurement of a change in the pressure of the gas, products in the gas phase were also analyzed by GC. CO adsorption on $Rh(C_3H_5)/SiO_2$ was also measured at RT under 20 kPa of CO.

XPS Measurements. XPS spectra were recorded on a Rigaku XPS-7000 apparatus at a base pressure of 9×10^{-8} Pa. The X-ray source, voltage, and current were Mg Kα, 10 kV, and 30 mA, respectively. Each sample was pressed to a thin disk for the measurement. Binding energies were referred to Si 2p (103.4 eV).

^{29}Si Solid-State MAS NMR Measurements. ^{29}Si solid-state MAS NMR spectra were measured on a Chemagnetics CMX-300 spectrometer operating at 59.68 MHz. Single-pulse detection method with hydrogen decoupling was used, where the pulse duration was 1.5 μs (corresponding to about $\pi/6$ pulse). The rotor spin rate was 4 kHz, with a delay time of 20 s. The accumulated numbers were fixed about 5000 for all samples. Chemical shifts are in ppm relative to tetramethylsilane fused in a glass tube as an external standard.

Peak signals attributed to the SiO_2 support were determined with the following procedure. The peak area of each sample depends on the amount of the sample and the acquisition time. First of all, the ratio of Si species corresponding to be Aerosil 200 support was estimated from the real change in the weight of the imprinted material and the calcinations at the high temperatures. Then, considering the ratio and the sample amount

TABLE 1: Gas-Phase Analysis of Propene and Propane in the Formation and Treatment of $Rh(C_3H_5)/SiO_2$[a]

entry	sample	condition	product	amount per Rh
(a)	$Rh(C_3H_5)_3$	attachment on SiO_2	C_3H_6	1.97
(b-1)	$Rh(C_3H_5)/SiO_2$	reaction with the amine in ethanol	C_3H_6	0.81
(b-2)		subsequent treatment with H_2 at 423 K[b]		0[c]
(c)	$Rh(C_3H_5)/SiO_2$	reaction with ethanol	C_3H_6	0.28
(d)	$Rh(C_3H_5)/SiO_2$	reaction with the amine in toluene	C_3H_6	0.12

[a] Products were analyzed by gas chromatography. [b] H_2: 30 kPa. [c] No product.

for the NMR measurement, the measured spectrum of Aerosil 200 evacuated at 773 K was calculated to be the Si species of Aerosil 200 including the sample. Finally, the spectrum of the sample subtracted from that of the support, and the obtained spectrum corresponding to the SiO_2−matrix overlayers were presented in a same figure.

ESR Measurements. X-band ESR spectra were recorded on a JES-RE2X apparatus. Each sample was enclosed in a quartz ESR cell under nitrogen atmosphere and evacuated at RT for 1 h. The measurement was performed at 10 K cooled by liquid helium.

EXAFS Measurements. EXAFS spectra at Rh K-edge were measured in a transmission mode at 15 K at the BL-10B station of the Photon Factory in the Institute of Materials Structure Science, High Energy Accelerator Research Organization (KEK-IMSS-PF) (Proposal No.: 2001G315). The energy and current of electrons in the storage ring were 2.5 GeV and 250−400 mA, respectively. X-rays from the storage ring were monochromatized by a Si(311) channel cut crystal. Ionization chambers filled with pure Ar and Kr gases were used to monitor the incident and transmitted X-rays, respectively. The EXAFS spectra were analyzed with the UWXAFS package.[25] The threshold energy E_0 was tentatively set at the inflection point of the absorption edge. The background was subtracted by the AUTOBK program. The k^3-weighed EXAFS data were Fourier transformed into *R*-space. The curve-fitting analysis was carried out using the FEFFIT program in the *R*-space.[26] The fitting parameters were coordination numbers (CN), interatomic distances (R), Debye−Waller factors (σ), and a correction-of-edge energy (ΔE_0). The phase shifts and backscattering amplitudes were calculated by the FEFF8 code.[26] The coefficient of the multiphoton effect (S_0^2) was fixed as 1.0 for the fitting.

Rh Loadings. Rh loading was determined by ICP (Hitachi P-4010). Rh samples were dissolved in a HF solution and heated for 10 min. Then the solution was diluted with distilled water after masking of HF by a H_3BO_3 solution.

DFT Calculation for the Attached Rh Complexes. Density functional calculation was performed using Dmol3 4.2.1[27] on a Cerius 2.4.2 graphical interface (Accelrys, USA). In all the calculations, spin−orbitals were restricted. The numerical basis set DNP was adopted, which is of double-ζ plus polarization functions quality. The orbitals included in the calculations were 1s and 2s for hydrogen, 1s, 2s, 2p, 3d for carbon, nitrogen, and oxygen atoms, 1s, 2s, 2p, 3s, 3p, 3d for silicon atoms, 4s, 4p, 4d, 5s, 5p for rhodium atoms. The criteria for the convergence of electronic states was 1.0×10^{-5} for the rms change in the norm of the electron density matrix. For the exchange-correlation functional, the nonlocal general gradient approximation given by Perdew and Wang was used through all the SCF cycles.[28] Structural optimization was performed by the DIIS algorithm and the criteria for convergence was 0.05 kcal mol^{-1} in this study.

Catalytic Hydrogenation of α-Methylstyrene. Each sample was suspended in a toluene solution under 101.3 kPa of H_2 in a closed batch reactor equipped with a mechanical stirrer. The Rh_{imp-a} complex was used as a catalyst after the evacuation at 373 K in the same reactor. Hydrogenation was initiated at 348 K by addition of neat α-methylstyrene to the suspension (Rh/α-methylstyrene/toluene = 1:4000:80000 in a molar ratio). The reactions were monitored by GC at an appropriate interval.

The inhibition of the hydrogenation was performed by using seven amines with different sizes and shapes in order to compare shape-selective behaviors on the imprinted Rh monomer. Benzylamine, the template α-methylbenzylamine, α,4-dimethylbenzylamine, 1-methylheptylamine, 1-methyl-3-phenylpropylamine, benzhydrylamine, and 1-(1-naphthyl)ethylamine were used as inhibitors for the reaction. A concentrated toluene solution of each amine inhibitor was added to the reaction phase, and decreases in the hydrogenation rate were monitored by GC. The change in the volume of the additional solvent corresponds to 0.6% of the reaction solution, and its effect can be disregarded.

3. Results

Attachment of the $Rh(\eta^3\text{-}C_3H_5)_3$ Precursor on a SiO_2 Surface. During the reaction between $Rh(\eta^3\text{-}C_3H_5)_3$ and SiO_2, all products were trapped and analyzed by GC. The results of the analysis are summarized in Table 1. C_3H_6 was only a product in the first attaching step, and the amount was estimated to be 1.97 C_3H_6 per Rh (Table 1 (a)). Accompanied with a change in the color of the sample, consequently $Rh(\eta^3\text{-}C_3H_5)_3$ was attached on the surface evolving two C_3H_6 in gas phase, while one C_3H_5 remained on Rh. The loading of the attached Rh species assessed by ICP shows that all $Rh(\eta^3\text{-}C_3H_5)_3$ precursors used in the step are attached on the surface. The same behaviors were observed in the Rh-loading range 0.2−0.6 wt %. The ν_{CH_2} and δ_{CH_2} of $\eta^3\text{-}C_3H_5$ are reported at 3055 cm^{-1}, 3000−2800 cm^{-1}, 1491 cm^{-1}, and 1463 cm^{-1},[29−31] but no peaks were observed for $Rh(C_3H_5)/SiO_2$ by FT-IR because of the low Rh loading of our samples.

The adsorption of H_2 or CO molecules was carried out for the obtained $Rh(C_3H_5)/SiO_2$ at RT. The both molecules did not adsorb on the Rh at all, and neither ν_{CO} nor ν_{Rh-H} was observed. But the complex decomposed by a long exposure to H_2 at RT. The color of the sample changed gradually from yellow to gray (black), and the small amount of H_2 molecules adsorbed on the decomposed sample. Such decomposition was not observed under CO.

Figure 1 shows Rh K-edge EXAFS oscillations and their associated Fourier transforms measured at 15 K for the $Rh(\eta^3\text{-}C_3H_5)_3$ precursor and the $Rh(C_3H_5)$ attached on SiO_2, whose curve-fitting results are presented in Table 2. The coordination number (CN) of Rh−C interaction for $Rh(\eta^3\text{-}C_3H_5)_3$ is valued to be 6.7 (±0.9), indicating that the three C_3H_5 ligands of $Rh(\eta^3\text{-}C_3H_5)_3$ coordinate to the Rh center with bidentate character at 0.218 (±0.001) nm. Attended to the attachment, an EXAFS oscillation changed as shown in Figure 1 (2a). As the structure around Rh changes by the reaction of two coordinated C_3H_5 ligands of $Rh(\eta^3\text{-}C_3H_5)_3$ with two OH groups at the SiO_2 surface, Rh−C bonding with a remaining C_3H_5 ligand and Rh−O

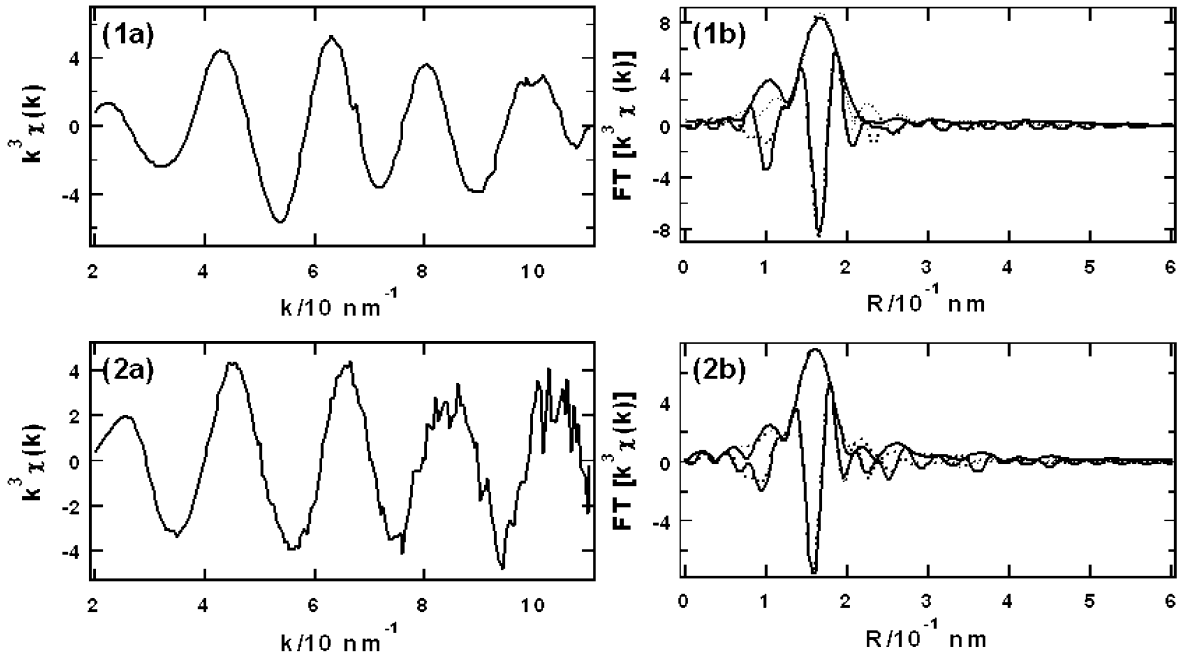

Figure 1. k^3-weighted Rh K-edge EXAFS oscillations (a) and their associated Fourier-transformed functions (b) for (1) Rh(η^3-C_3H_5)$_3$ and (2) Rh(C_3H_5)/SiO_2 measured at 15 K. Two solid lines and dotted lines in (b) represent the absolute values and imaginary parts of the observed data (solid) and the fitted spectra (dotted), respectively.

TABLE 2: Curve-Fitting Results of Fourier-Transformed EXAFS Functions for Rh(C_3H_5)$_3$ and Rh(C_3H_5)/SiO_2 Measured at 15 K

shell	CN	distance /nm	σ^2 /nm^2
Rh(C_3H_5)$_3$[a]			
Rh−C	6.7 ± 0.9	0.218 ± 0.001	(3 ± 1) × 10^{-5}
Rh(C_3H_5)/SiO_2[b]			
Rh−C	2.0[c]	0.218[c]	3 × 10^{-5} [c]
Rh−O	1.7 ± 0.3	0.205 ± 0.001	(1 ± 2) × 10^{-5}

[a] k = 3−11, r = 1.1−2.0, R_f = 0.84%. [b] k = 3−11, r = 1.1−2.0, R_f = 1.21%. [c] Fixed.

bonding with two surface oxygen atoms should be observed. Therefore, the curve fitting of the Fourier-transformed function was performed by Rh−C and Rh−O shells. Since free fitting by the two shells of Rh−C and Rh−O is not permitted because the allowed free parameters are only 6 estimated by Nyquist's law,[32] and Rh−C and Rh−O bonds cannot be discriminated from each other by EXAFS,[33] the structural parameters for Rh−C were fixed on the basis of the experimental fact (Table 2). The determined bond at 0.205 nm is assumed as Rh−O, which is much shorter than the Rh−C bond of 0.218 nm. The coordination number of the Rh−O bond was 1.7 ± 0.3, which indicates the coordination of two surface oxygen atoms to a Rh atom as shown in Figure 2.

An XPS spectrum for Rh(C_3H_5)/SiO_2 is shown in Figure 3. The binding energies of the attached Rh(C_3H_5) species and some references are summarized in Table 3. The attached Rh complex decomposes during the XPS measurement, and the color of the resultant sample changed from golden yellow to black. The same phenomenon was reported by Foley et al., and the decomposition started from the initial stage of the XPS measurement.[29] In their report, the Rh 3d binding energy was initially 308.9 eV and decreased gradually to 308.0 eV after 90 min. The value in our 90-min measurement was 308.2 eV, where the similar reduction in the binding energy during the measurement is suggested. The Rh loading in our samples was quite low because of the imprinting on the surface, and we could not know the real binding energy in the early stage of the XPS measurement.

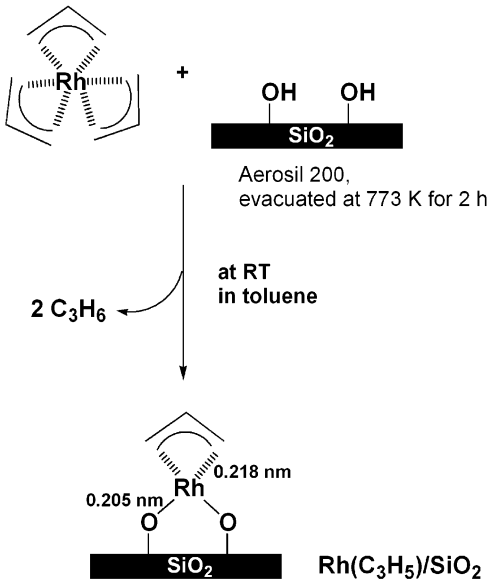

Figure 2. The attachment of Rh(η^3-C_3H_5)$_3$ on a SiO_2 surface.

Neutral Rh metals have a much smaller binding energy like 307.0 eV, and Rh(I) compounds have the values in the range 307.4−308.8 eV and they do not exceed 308.9 eV as shown in Table 3. Therefore, the reported initial value of 308.9 eV indicates that the valance of the Rh species is neither 0 nor 1+. On the other hand, a Rh 3d level of Rh(II) acetate dimer is 308.8 eV, and those of Rh(III) compounds widely range from 308.7 eV (Rh_2O_3) to 310.5 eV ([Rh(NH_3)$_6$]Cl_3) as shown in Table 3. Hence the oxidation state of the attached Rh species is 2+ or 3+. Rh^{2+} ions should be detected by ESR, but no peak signals were observed even at 10 K, indicating that there is no Rh^{2+} species in the Rh(C_3H_5)/SiO_2. The XPS and ESR data also reveal the Rh^{3+} complex attached on SiO_2 in Figure 2.

Preparation of an Amine-Coordinated Rh Complex (Rh_{sup}) on SiO_2. In the second step to coordinate amine ligands as a

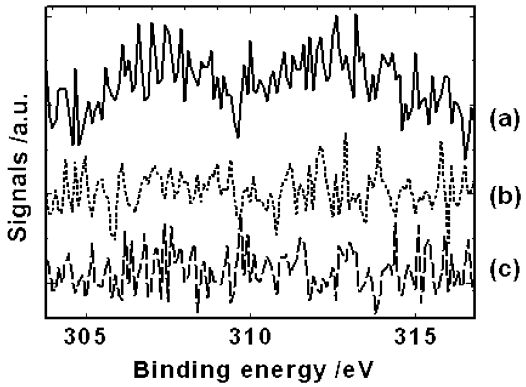

Figure 3. Rh $3d_{5/2}$ and $3d_{3/2}$ XPS spectra for (a) Rh_{sup} (solid), (b) Rh_{imp-b} (dotted), and (c) Rh_{imp-a} (broken) samples. The spectra are noisy due to the low Rh loading, but the difference between them is obvious.

TABLE 3: XPS Binding Energies for the Rh Complexes and Some References

sample	Rh 3d binding energy /eV	Rh valance	reference
$Rh(C_3H_5)/SiO_2$	308.9[a]		29
	308.0[b]		29
$Rh(C_3H_5)/SiO_2$	308.2[c,d]		this study
Rh_{sup}	308.1[d]		this study
Rh_{imp-b}	- - -		this study
Rh_{imp-a}	- - -		this study
Rh metal	307.0	0	38
$RhCl(PPh_3)_3$	307.4	1	39
$RhCl(CO)(PPh_3)_2$	308.7	1	40
$Rh_2Cl_2(C_2H_4)_2$	308.8	1	41
$Rh_2(CH_3COO)_4$	308.8	2	42
Rh_2O_3	308.7, 309.1	3	43, 38
$RhCl_3(PPh_3)_3$	309.7	3	44
$RhCl_3$	310.0	3	38
$[Rh(NH_3)_6]Cl_3$	310.5	3	45

[a] Measured for 5 min. [b] Measured for 90 min. [c] Decomposition was observed after a measurement for 90 min. Similar phenomenon was reported by Foley et al. [29]. [d] These values are referred to Si 2p and O 1s (SiO_2), 103.4 and 533.0 eV, respectively.

template to the attached Rh complex, the analysis of products was also performed, and the results are summarized in Table 1. C_3H_6 was evolved as a major product, and the amount of C_3H_6 detected by GC was 0.81 per Rh (Table 1 (b-1)), which supports the existence of a remaining C_3H_5 ligand on a Rh atom in the $Rh(C_3H_5)/SiO_2$ sample. Further, by the treatment of the obtained Rh_{sup} complex at 423 K under H_2, no products derived from C_3H_5 were observed though C_3H_6 or C_3H_8 would be produced if the C_3H_5 ligand had not completely substituted with the amine (Table 1 (b-2)).

To know the detail of the reaction of the $Rh(C_3H_5)/SiO_2$ with amine, the analysis of products was also conducted under other reaction conditions. In the absence of the template amine, the small amount of C_3H_6 per Rh was formed after the reaction in ethanol for 1 h (Table 1 (c)). In toluene, such a color change was not observed, and C_3H_6 formation was hardly formed (Table 1 (d)). Judging from all the results of the C_3H_6 formation, the coordination of the amine ligand to the Rh atom proceeds in cooperation of ethanol, reducing the C_3H_5 ligand to generate C_3H_6. The amine coordination is suggested to be a reductive pathway promoted by ethanol.

The Rh 3d XPS binding energy for Rh_{sup} was 308.1 eV as shown in Table 3 and Figure 3. No decomposition occurred with the Rh_{sup} complex. The value evidences that the Rh^{3+} species of $Rh(C_3H_5)/SiO_2$ was reduced during the reaction with the amine in ethanol. Any ESR signal was not observed at 10 K, indicating no Rh^{2+} species involved in the sample. Hence the Rh−amine complex on SiO_2 is considered to be a Rh^{1+} complex.

TABLE 4: Curve-Fitting Results of Fourier-Transformed EXAFS Functions for the Supported and Imprinted Rh Catalysts Measured at 15 K

shell	CN	distance /nm	σ^2 /nm^2
Rh_{sup}			
Rh−N[a]	4.2 ± 0.5	0.212 ± 0.001	$(3 \pm 1) \times 10^{-5}$
Rh_{imp-b}			
Rh−N[b]	3.8 ± 0.3	0.209 ± 0.001	$(3 \pm 1) \times 10^{-5}$
Rh_{imp-a}			
Rh−N[c]	3.2 ± 0.3	0.205 ± 0.001	$(1 \pm 1) \times 10^{-5}$

[a] $k = 3-11$, $r = 1.1-2.0$, $R_f = 0.64\%$. [b] $k = 3-11$, $r = 1.1-2.0$, $R_f = 0.33\%$. [c] k = 3−11, $r = 1.1-2.0$, $R_f = 0.42\%$.

The structure of the Rh_{sup} complex was determined by EXAFS. Figure 4 (1) shows an EXAFS oscillation and its associated Fourier transformed function for the Rh_{sup} complex. It was fitted by a Rh−N shell (N and O cannot be discriminated by EXAFS), whose curve-fitting parameters are shown in Table 4. The CN and R of Rh−N were estimated to be 4.2 (± 0.5) and 0.212 (± 0.001) nm, respectively. The reaction in ethanol required two amine ligands per Rh, and there was no significant change in the EXAFS spectrum by the addition of more than two amines to the system. It is suggested that two amines coordinate to a Rh atom and that the Rh atom is bound to the SiO_2 surface through Rh−O bonds in a bidentate form. According to these results, the surface structure of the Rh−amine complex (Rh_{sup}) is illustrated as structure B in Figure 5.

Stacking of SiO_2−Matrix Overlayers on the Rh_{sup} Surface. The molecular imprinting of the Rh_{sup} complex attached on Aerosil 200 SiO_2 surface was conducted by the hydrolysis−polymerization of $Si(OCH_3)_4$. Both $Si(OCH_3)_4$ and H_2O were deposited on the surface by a chemical vapor deposition method. At RT, the hydrolysis of the deposited $Si(OCH_3)_4$ did not react efficiently, and the majority of $Si(OCH_3)_4$ evaporated by the following evacuation. At higher temperatures than 363 K, the hydrolysis−polymerization proceeded completely, but the template amine ligand dissociated during the hydrolysis−polymerization. Thus, 333 K was found to be the best temperature, where the hydrolysis−polymerization proceeded on the surface without the loss of the template amine from the Rh site.

A large increase in a sample weight was observed after the hydrolysis−polymerization. The sample weight became 2.08 times larger than the weight of the SiO_2 support, which includes the support, the SiO_2 network formed by this hydrolysis, and physically adsorbed molecules (water, methanol, etc.). To estimate the portion of hydrolyzed $Si(OCH_3)_4$ in the sample, the Rh_{imp-b} sample was calcined at several temperatures and measured its weight after cooling to RT. The sample weights gradually reduced with an increase in the calcined temperature, and the final weight after the calcination at 773 K decreased to 93% of the original weight before the calcination. This corresponds to the sum of the support weight and the deposited SiO_2 weight. Thus, the portion of the Si species of the Aerosil 200 support was estimated to be 52% of the whole Si species in the sample, and 87% of $Si(OCH_3)_4$ employed in the deposition was hydrolyzed under the present condition.

Figure 6 shows ^{29}Si solid-state MAS NMR spectra for the imprinted Rh_{imp-b} sample (Figure 6 (a)) and a reference sample deposited with the same amount of $Si(OCH_3)_4$ on an Aerosil 200 without attached Rh complexes (Figure 6 (b)). A difference spectrum is shown by a dotted line. Three sharp peaks are attributed to Q_4 bulk Si species (−109 ppm), Q_3 (−99 ppm),

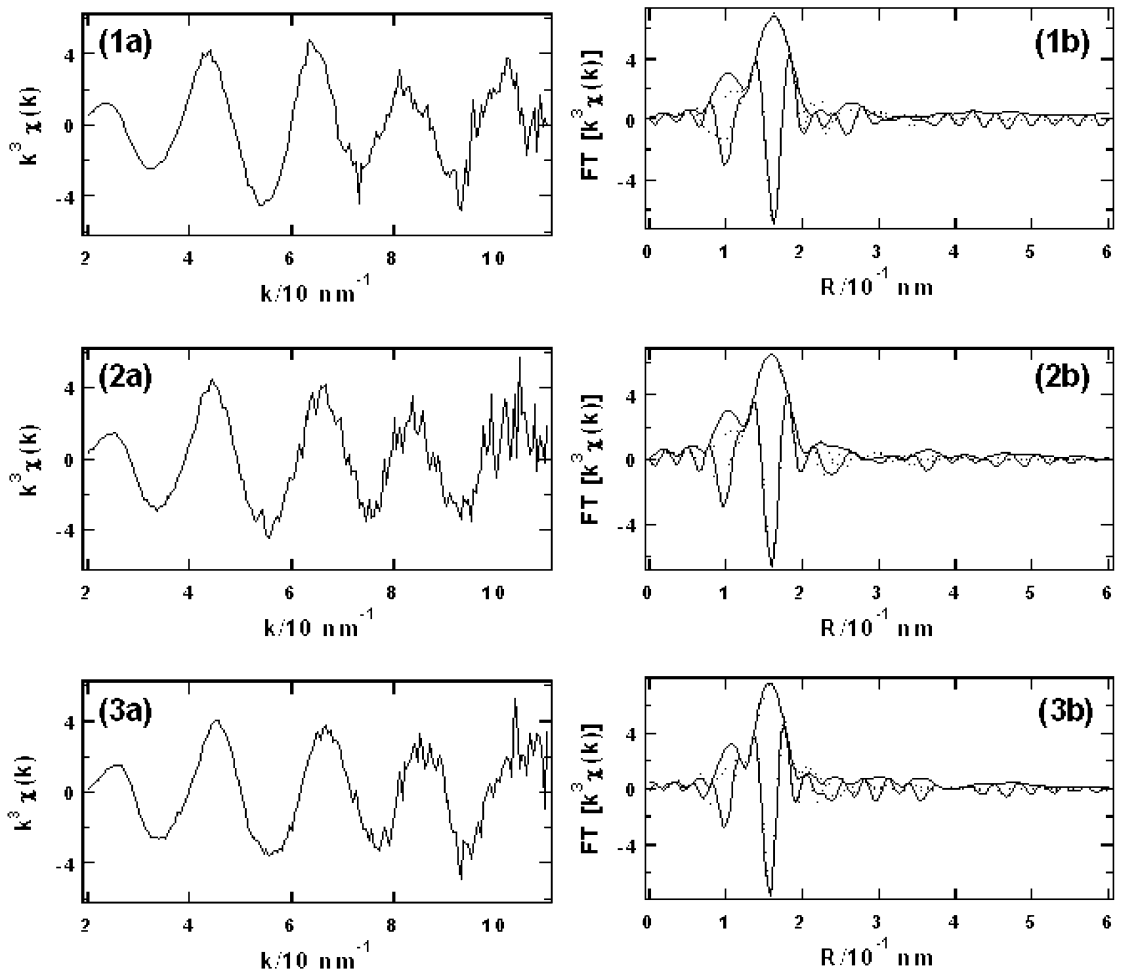

Figure 4. k^3-weighted Rh K-edge EXAFS oscillations (a) and their associated Fourier-transformed functions (b) for (1) Rh_{sup}, (2) Rh_{imp-b}, and (3) Rh_{imp-a} complexes. Two solid lines and dotted lines in spectra (b) represent the absolute values and imaginary parts of the observed data (solid) and the fitted spectra (dotted), respectively.

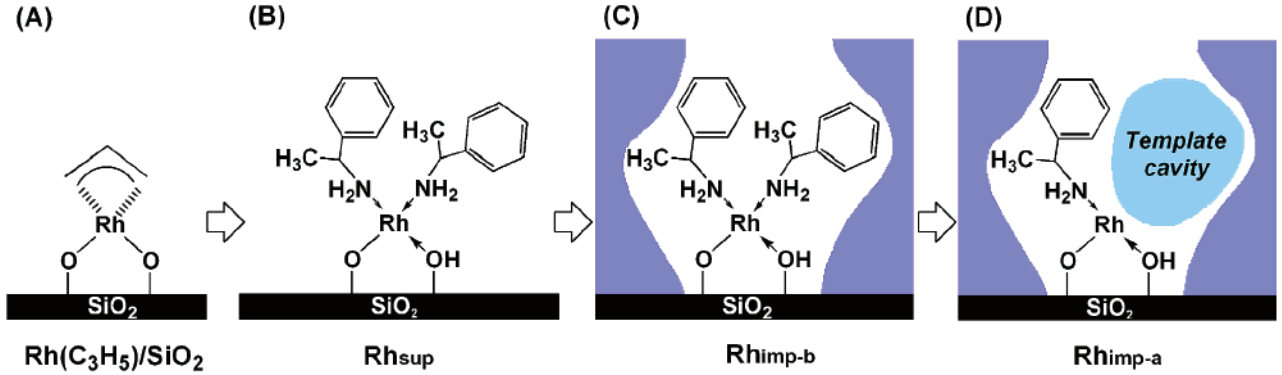

Figure 5. The preparation scheme for the imprinted Rh−amine complex on a SiO_2 surface.

and Q_2 (−91 ppm) surface Si species. This indicates that the deposited $Si(OCH_3)_4$ forms a SiO_2 network under the present condition.

From the comparison between the spectra for the two samples with and without the attached Rh−amine complexes, we can see significant differences between them. In the absence of Rh, the peak intensity of Q_3 ($Si(OH)(OSi)_3$) is the same as that of Q_4 ($Si(OSi)_4$), and Q_2 ($Si(OH)_2(OSi)_2$) species also forms on the surface, indicating that the SiO_2 network has a lot of surface silanol groups. The results are similar to those on Ox.50 support.[6−8]

In contrast, in the case of Rh_{imp-b} sample, Q_4 is major, and surface Q_3 species and in particular Q_2 species are minor as shown in Figure 6 (a). The similar results were observed on Ox.50 with the Rh-amine complexes prepared as a reference, irrespective of a kind of SiO_2 support. Such an increase in the Q_4 quantity was not observed in the case of SiO_2-attached Rh−phosphite complexes.[6,7] Thus it is suggested that the amine ligands promote the hydrolysis−polymerization of $Si(OCH_3)_4$. There are not extra amines on the surface, and hence the hydrolysis−polymerization proceeds to form a SiO_2 network around the attached Rh−amine complexes. Many Q_3 species

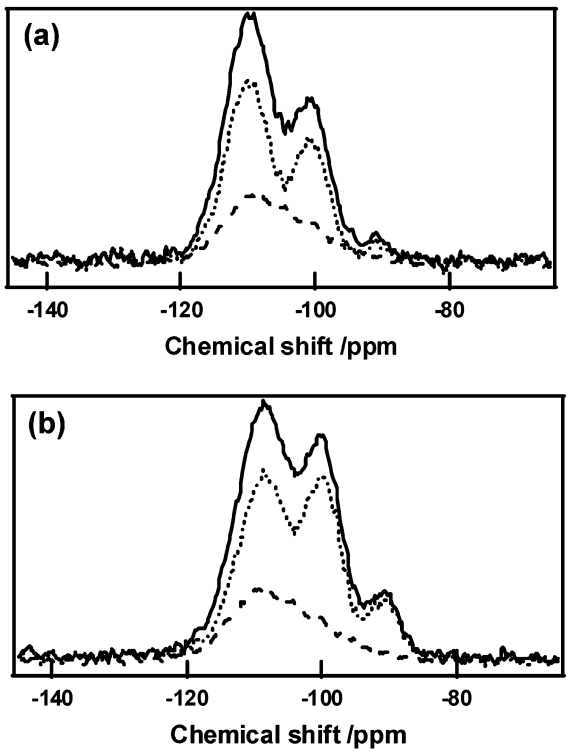

Figure 6. ^{29}Si solid-state MAS NMR spectra for (a) Rh_{imp-b} and (b) a reference prepared without attached Rh complexes. Solid, dashed, and dotted lines represent the spectrum of the samples, that of Aerosil 200 (support), and the difference spectrum corresponding to the SiO_2−matrix overlayers, respectively.

remain in the sample as shown in Figure 6 (a), which makes the SiO_2 network sufficiently flexible to model into the shape of the template.

A Rh 3d XPS spectrum changed dramatically after the imprinting as shown in Figure 3 (b), where no significant contribution of Rh 3d was observed. This indicates that the attached Rh−amine complexes were surrounded by the SiO_2−matrix overlayers on the surface. Similar behavior was observed on the imprinted Rh−phosphite complexes on Ox.50.[6,7] Although the oxidation state of Rh cannot be determined by XPS. There is no reason to oxidize or reduce during the hydrolysis−polymerization. Indeed no ESR signals were observed at 10 K, suggesting no change in the Rh^{1+} monomer.

Figure 4 shows a Rh K-edge EXAFS oscillation (2a) and its associated Fourier transformed function (2b) for the Rh_{imp-b} complex. The curve-fitting result presented in Table 4 reveals that the attached Rh complex maintains its original structure after the stacking of the SiO_2−matrix overlayers. The CN and R fitted by a Rh−N shell were 3.8 (±0.3) and 0.209 (±0.001) nm, respectively. Judging from the ESR and EXAFS, the conformation of Rh_{imp-b} is the same as that of Rh_{sup} as shown in Figure 5 (structure (C)); that is, no ligands are eliminated from the attached Rh species during the hydrolysis−polymerization within the experimental error.

Removal of the Template Amine Ligand from the Attached Rh Complex. The final step for the molecular imprinting is the removal of the template amine ligand from the attached Rh monomer. To eliminate the template amine ligand, evacuation conditions were optimized in the temperature range 293−423 K. Lower temperature cannot extract any ligands, while evacuation at higher temperature like 423 K causes the decomposition of Rh complex. The best temperature to eliminate only one amine ligand as the template is 373 K.

ESR measurements for the obtained Rh_{imp-a} sample revealed no peak signals. Further, there was no XPS peak as shown in Figure 3 (c). These results suggest no significant change in the oxidation state and the location of the Rh atom in the process of the formation of the Rh_{imp-a} sample.

The amount of adsorbed H_2 molecules per Rh_{imp-a} was 0.9 at 80 kPa, indicating that all the Rh complexes locate on the support surface without being buried by the SiO_2−matrix overlayers. The H_2 adsorption was reversible and had linear dependency against H_2 pressure.

The removal of one amine ligand was confirmed by Rh K-edge EXAFS. The EXAFS oscillation and its associated Fourier-transformed function are shown in Figure 4 (3). The structural parameters are given in Table 4. The CN and R fitted by a Rh−N shell was 3.2 (±0.3) and 0.205 (±0.001) nm, respectively. The CN decreased approximately from 4 to 3, which suggests the elimination of one amine ligand by the evacuation of the Rh_{imp-b} sample at 373 K. The shortening of *R* from 0.209 to 0.205 nm means a stronger interaction between the Rh center and the remaining ligand because of the unsaturated Rh state. The structure of the Rh_{imp-a} complex is illustrated in Figure 5 (structure D). Attended to the removal of an amine ligand as the template, a template-shaped cavity is created on the Rh center behind the template. The elimination of one of two amine ligands is also evidenced by the following DFT modeling of the Rh monomer on a SiO_2 cluster model.

To understand the removal step of the template, five models of attached Rh complexes on a small SiO_2 cluster support were calculated by the DFT theory. An energy profile for the models is presented in Figure 7. The initial Rh_{sup} complex with two amine ligands ($Rh(Amine)_2(O-Si)(HO-Si)$) is structure (a); a Rh complex with a monodentate silanol ($Rh(Amine)_2(O-Si)$) is denoted as structure (b); the Rh_{imp-a} complex with one amine ligand produced by the removal of an amine ligand of structure (a) ($Rh(Amine)(O-Si)(HO-Si)$) is structure (c); another possible complex with an amine ligand ($Rh(Amine)(O-Si)(HO-Si)$) different from structure (c) is denoted as structure (d); a bare Rh species without any amine ligand ($Rh(O-Si)(HO-Si)$) is structure (e). The same SiO_2 cluster unit was used for all the modeling, but the whole system including the SiO_2-cluster unit was optimized energetically in the DFT calculation. There are two energy levels for the Rh_{imp-a} complexes with one amine ligand (c) and (d), and the lower energy path with 31 kcal mol^{-1} from Rh_{sup} (a) to Rh_{imp-a} (c) is shown in Figure 7. The other Rh structure (d) with the same composition, but with another amine ligand is 7 kcal mol^{-1} less stable than structure (c). The value of energy difference depended a little on the asymmetry of the bidentate bonding from the SiO_2 support (Si−O and Si−OH), and the more stable structure (c) in the real system seems to form preferably. The energy level of structure (b) was 18 kcal mol^{-1} higher than that for the initial state (a). Hence the population of structure (b) is negligible under the evacuation condition. The irreversible elimination of an amine ligand ((a) → (c)) at 373 K is a kinetically controlled process. There is a 74 kcal mol^{-1} energy barrier from structure (a) to structure (e) as shown in Figure 7. The value is too large to reach the state of bare structure (e). Thus the Rh_{imp-a} complex on the surface (structure (c)) is preferably designed with the preparation procedure (D in Figure 5).

Catalytic Hydrogenation of α-Methylstyrene. Table 5 represents reaction results of α-methylstyrene hydrogenation on four catalysts $Rh(C_3H_5)_3$, $Rh(C_3H_5)/SiO_2$, Rh_{sup}, and Rh_{imp-a}. A half-hydrogenated species of α-methylstyrene has size and shape similar to those of the template amine, α-methylbenzyl-

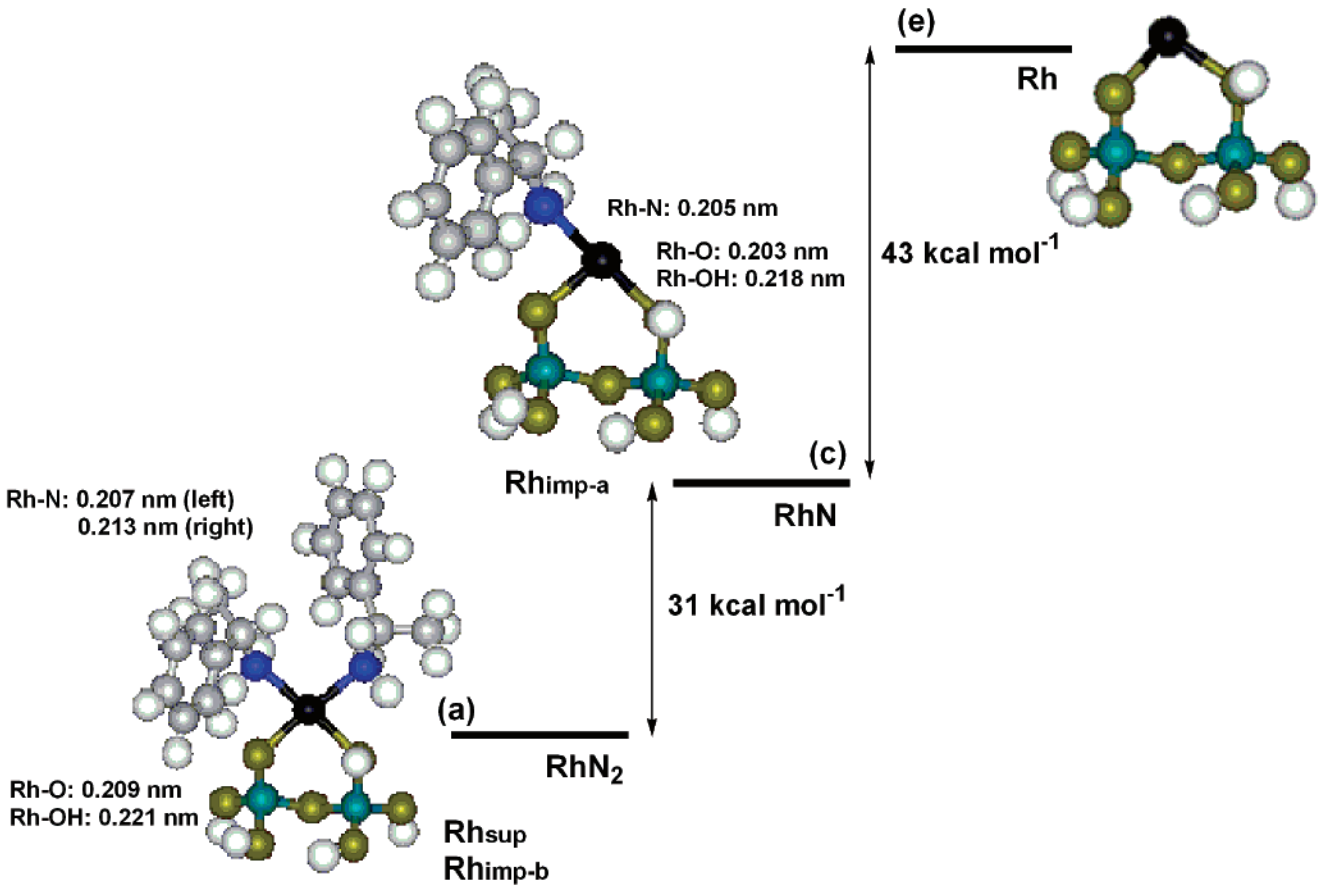

Figure 7. An energy profile for several models of attached Rh complexes calculated by DFT.

TABLE 5: Catalytic Activities for α-Methylstyrene Hydrogenation[a]

catalyst	TOF/min^{-1}
$Rh(C_3H_5)_3$	0[b]
$Rh(C_3H_5)/SiO_2$	0[b]
Rh_{sup}	0[b]
Rh_{imp-a}[c]	5.2

[a] H_2 101.3 kPa, at 348 K, in a toluene solution, Rh/α-methylstyrene/toluene = 1/4000/80000 (in a molar ratio). [b] Decomposition was observed under the reaction condition. The values are initial rates. [c] After evacuation at 373 K for 3 h.

amine. The $Rh(C_3H_5)_3$ precursor, the attached $Rh(C_3H_5)/SiO_2$, and the Rh_{sup} complex with two amine ligands showed no catalytic activity for the reaction at 348 K. Furthermore, they easily decomposed to metal aggregates under the reaction conditions. On the other hand, the Rh_{imp-a} complex exhibited a remarkable catalytic activity for the hydrogenation (Table 5). The turnover frequency (TOF) of Rh_{imp-a} is 5.2 min^{-1}, whereas the other structures are not active at all. The imprinted catalyst was also durable for the reaction.

Figure 8 shows the relationship between the TOFs and the evacuation temperature. On the Rh_{imp-b} complex evacuated at 333 K, the TOF was so small as 0.9 min^{-1}. Accompanied with increasing evacuation temperature, the catalytic activity increased, and the maximum activity was observed in the range of evacuation temperature 363−383 K as shown in Figure 8. Further increase in the temperature caused a decrease in the activity, and the evacuation at 423 K reduced the reaction rate to half (Figure 8) due to the decomposition of the Rh complexes.

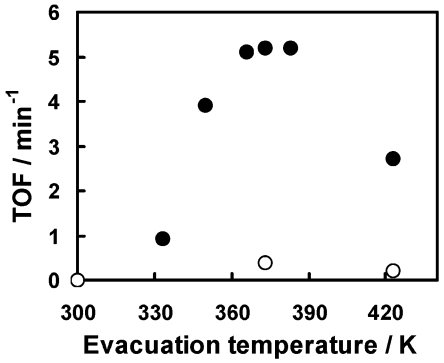

Figure 8. The change in catalytic activity for α-methylstyrene hydrogenation at 348 K with the pretreatment at various temperatures under vacuum. Black circles and white circles represent TOFs of the Rh_{imp} complex and TOFs of the Rh_{sup} complex, respectively.

Thus, the best temperature 373 K for evacuation was adopted to eliminate the template and to prepare the active Rh_{imp-a} complex.

The turnover number (TON) against the reaction time is shown in Figure 9. The hydrogenation proceeds linearly on the imprinted Rh_{imp-a} catalyst, and the loss of the catalytic activity was not observed during a prolonged reaction. In contrast, the initial activity of the Rh_{sup} catalyst was zero, and then the reaction occurred accompanied with the decomposition of the Rh complex, but the activity lost finally (Figure 9).

Shape-Selective Inhibition of α-Methylstyrene Hydrogenation by Seven Amines with Different Shapes. The inhibition of the α-methylstyrene hydrogenation by several amines with different shapes revealed shape-selective aspects on the designed

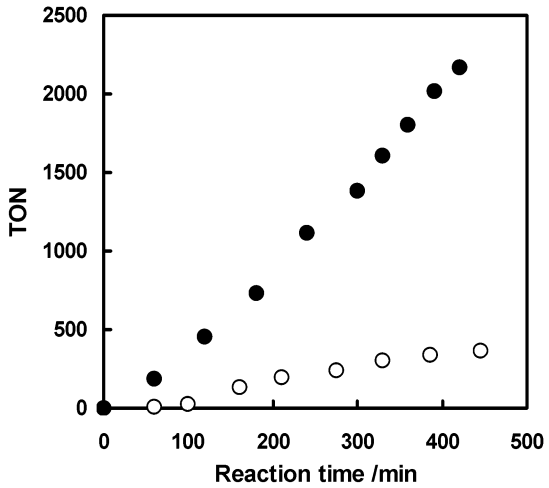

Figure 9. TONs for α-methylstyrene hydrogenation at 348 K on the Rh_{imp-a} complex (black circles) and the Rh_{sup} complex (white circles) as a function of reaction time.

Rh_{imp-a} complex as shown in Figure 10. The degrees of the inhibition and some remarks for their shapes are summarized in Table 6.

The inhibitions showed a linear dependency on the concentration of each amine, but there were large differences in the degree of inhibition among seven amine inhibitors. The smaller benzylamine (Inh. 1) and the template α-methylbenzylamine (Inh. 2) have similar dependency to each other as shown in Figure 10. They required about 4 equivalent to Rh to reduce the reaction rate to half (Table 6). On the other hand, larger inhibitors (Inh. 3−7) showed different behaviors as to their sizes and shapes. α,4-dimethylbenzylamine (Inh. 3) is larger by a methyl group than the template (Inh. 2). The significant difference in the inhibition degrees was observed in Figure 10. The template (Inh. 2) and 1-methylheptylamine (Inh. 4) with a long alkyl chain possess the same number of carbon atoms, but the long 1-methylheptylamine inhibits the reaction more weakly than the template. The amount of Inh. 4 to reduce the activity to half was twice of that of Inh. 2 (template) as shown in Table 6. The comparison between the template (Inh. 2) and 1-methyl-3-phenylpropylamine (Inh. 5) shows the effect of an inner ethyl chain connecting a phenyl ring. The difference was also significant as shown in Figure 10. Benzhydrylamine (Inh. 6) and 1-(1-naphthyl)ethylamine (Inh. 7) have another phenyl ring on the carbon center next to the nitrogen atom and a naphthyl ring instead of a phenyl ring, respectively (Figure 10). Their amounts necessary to reduce the rate to half were 2.3 and 3.4 times larger than that for the template, respectively, (Table 6). In particular, Inh. 7 with a large naphthyl group was most inefficient for the inhibition, indicating that the Inh. 7 amine is hard to enter the template cavity and coordinate to the Rh site.

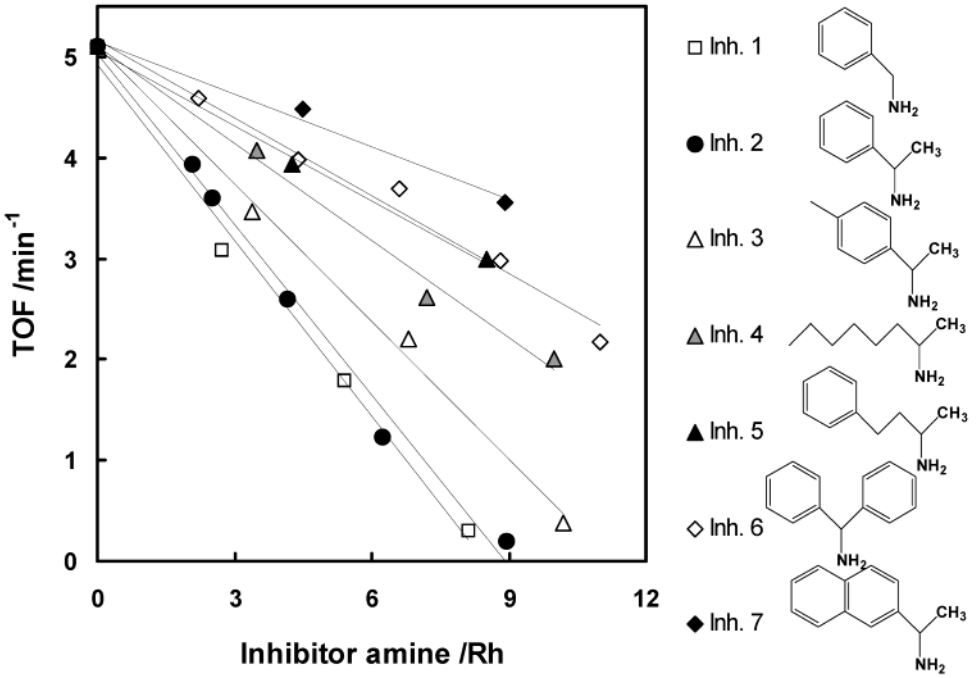

Figure 10. The inhibition of α-methylstyrene hydrogenation at 348 K by seven amine inhibitors with different shapes. The changes in TOFs by the inhibitors are plotted against the amounts of amines per Rh.

TABLE 6: Degrees of Inhibition for α-Methylstyrene Hydrogenation on the Rh_{Imp-a} Complex by the Seven Amine Inhibitors[a]

entry	amine inhibitor	shape	amine/Rh[b]
Inh. 1	benzylamine	small (1 Me)	4.1
Inh. 2	α-methylbenzylamine	the template	4.4
Inh. 3	α,4-dimethylbenzylamine	large (1 Me on the Ph group)	5.6
Inh. 4	1-methylheptylamine	large (long alkyl chain)	8.0
Inh. 5	1-methyl-3-phenylpropylamine	large (Et chain to Ph)	10.1
Inh. 6	benzhydrylamine	large (one more Ph group)	10.2
Inh. 7	1-(1-naphthyl)ethylamine	large (1 naphthyl group)	15.0

[a] H_2 101.3 kPa, at 348 K, in a toluene solution, Rh/α-methylstyrene/toluene = 1/4000/80000 (in a molar ratio). [b] The values are the required amounts of inhibitor amines to reduce the reaction rates to half.

4. Discussion

Preparation of the Template-Coordinated Rh Monomer (Rh_{sup}) on the SiO_2 Surface. Many metal−C_3H_5 complexes react with surface hydroxyl groups of oxides to be immobilized on the surfaces.[1−3,29−31,34−37] $Rh(\eta^3\text{-}C_3H_5)_3$ is easily attached on SiO_2 releasing C_3H_6, but several attached Rh structures have been proposed.[29−31,35,36] Hence we carefully examined the Rh structure attached on SiO_2 surfaces. On Aerosil 200 evacuated at 773 K, two propene molecules are evolved by the impregnation of $Rh(\eta^3\text{-}C_3H_5)_3$ in toluene as shown in Table 1, which indicates the stoichiometric reaction of a $Rh(\eta^3\text{-}C_3H_5)_3$ precursor with two surface silanol groups as shown in Figure 2. The number of evolved C_3H_6 agrees with the result reported by Foley et al.[29] The stoichiometric formation of propene was observed in the Rh-loading range 0.2−0.6 wt %. The attached Rh complexes did not adsorb H_2 and CO, and any vibrations attributed to Rh−H and Rh−CO were not detected by FT-IR. This indicates that there are no other Rh species with unsaturated structures, e.g., bare Rh species without C_3H_5 ligand, under our experimental conditions. This is contrasted to the case of higher Rh loading conditions, where a mixture of different structures involving a bare Rh species that can adsorb both CO and H_2 are produced.[29] In our case, the Rh loading is regulated to be low to separate sufficiently each other on the surface. Such dispersion is quite important for the molecular imprinting on the surface, which requires enough space to surround the attached Rh complex by surface-matrix overlayers. However, a 0.7 Rh wt % sample adsorbed the small amount of CO molecules (20% of total Rh), indicating inhomogeneous Rh species with this loading. According to the stoichiometric attachment on the surface and the resultant nearly uniform structure, the formal valance of the attached Rh species is concluded straightforwardly to be 3+. The results of XPS and ESR support this as described above.

The Rh K-edge EXAFS analysis is given in Table 2, where the determined CN and *R* (bond distance) of Rh−O are 1.7 ± 0.3 and 0.205 ± 0.001 nm, respectively. The EXAFS analysis also confirms the Rh atom attached on SiO_2 in a bidentate form $[Rh(C_3H_5)(OSi)_2]$ as shown in Figure 2. The similar Rh structure was reported on a TiO_2 surface.[37]

The next step is the coordination of an amine template to the attached Rh complex $[Rh(C_3H_5)(OSi)_2]$. α-Methylbenzylamine was chosen as a template ligand because it has a shape similar to that of a half-hydrogenated intermediate species in α-methylstyrene hydrogenation:

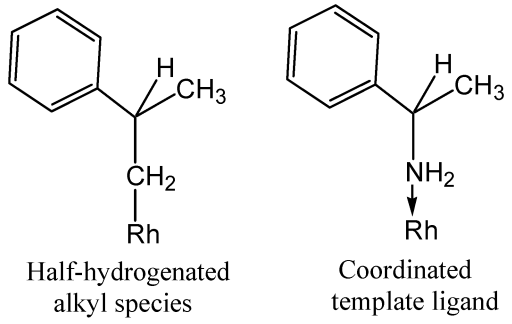

Half-hydrogenated alkyl species — Coordinated template ligand

Thus, the space behind the removal of the template will be a shape-selective reaction field. As many amine compounds are available, many kinds of shape-selective sites can be prepared in a similar way.

The template amine coordination was conducted in ethanol at RT. In this step, about one C_3H_6 per Rh generated (Table 1 (b-1)) and there was no remaining C_3H_5 ligand any more (Table 1 (b-2)), indicating that the stoichiometric reaction of C_3H_5 ligand with α-methylbenzylamine proceeded in ethanol at RT. The fact that C_3H_6 is produced from the C_3H_5 ligand demonstrates that the $[Rh(C_3H_5)(OSi)_2]$ species is reduced during the substitution of the C_3H_5 ligand with the amine template. However, only 12% of the C_3H_5 ligand was converted to C_3H_6 in toluene (Table 1 (d)), which indicates that the NH_2 group of α-methylbenzylamine does not contribute to it significantly. Ethanol used as the solvent for the amine coordination reduced the Rh species to form 0.28 C_3H_6 per Rh (Table 1 (c)). It is to be noted that the amine coordination quantitatively proceeds in the cooperation of ethanol and α-methylbenzylamine. The mechanism is not clear at the moment, but the amine coordination is explained by the following cooperative reaction pathway: (1) an ethanol molecule reacts with the C_3H_5 ligand to form C_3H_6 evolved in gas phase and an ethoxy ligand on Rh; (2) the ethoxy ligand is oxidized to acetaldehyde, while the Rh^{3+} species is reduced to coordinatively unsaturated Rh^+ species; (3) the Rh^+ species is coordinated with α-methylbenzylamine. Ethanol acts as a two-electron reducing reagent. The total reaction equation is given by $Rh(C_3H_5)(OSi)_2$ (Figure 5 (A)) + C_2H_5OH + 2 Amines → $Rh(Amine)_2(OSi)(HOSi)$ (Figure 5 (B)) + CH_3CHO + C_3H_6.

The detection of the produced acetaldehyde was attempted, but it was not successful by GC because the Rh loading was quite low and the produced acetaldehyde adsorbs on the surface. Instead, $Rh(\eta^3\text{-}C_3H_5)_3$ was attempted to react with the amine in ethanol, and plenty of acetaldehyde was detected by GC, supporting the above conclusion. However, the reaction in the homogeneous solution required high temperature and eventually decomposed; therefore, the Rh^+−amine complex is unique and prepared preferably on the surface. The Rh 3d XPS data confirm the reduction of the Rh complex from Rh^{3+} to Rh^{1+}. The observed binding energy (BE) of Rh 3d for the Rh_{sup} complex is 308.1 eV as given in Table 3, which is a typical BE of Rh^{1+} level. ESR excludes the possibility of bivalency.

The structure of the Rh_{sup} complex was finally determined by EXAFS. The Rh K-edge EXAFS spectrum at 15 K shows the existence of four Rh−N/O bonds around a Rh atom (CN = 4.2 ± 0.5) at the distance of 0.212 (± 0.001) nm. Further two amines were required for the completion of the transformation of $Rh(C_3H_5)/SiO_2$ (A) to the Rh_{sup} complex (B) at the surface, and excess amines did not change the structure (B) $Rh(Amine)_2$-(O−Si)(HO−Si) (Figure 5 (B)) anymore as proved by color change and EXAFS.

Preparation of the Amine-Imprinted Rh Monomer (Rh_{imp-a}) on the SiO_2 Surface. The third step of surface molecular imprinting is the stacking of SiO_2−matrix overlayers on the Rh_{sup} surface using $Si(OCH_3)_4$ as a polymerizing reagent. $Si(OCH_3)_4$ earned some excellent printing results in our previous studies:[6−8] (1) the stacking of SiO_2 network proceeds layer by layer to form SiO_2−matrix overlayers on a SiO_2 support; (2) $Si(OCH_3)_4$ reacts with surface silanol groups preferentially, and the polymerization does not occur in the absence of surface silanols under the present conditions; (3) as a result, the height of the matrix overlayers from the surface is controlled, pores including attached Rh complexes are produced in the SiO_2−matrix overlayers, and the attached Rh complexes are not buried in the surface−matrix overlayers; (4) the SiO_2 matrix possesses a lot of silanol groups (Q_3 and Q_2) to be flexible enough to shape the template figure. Therefore, we also chose $Si(OCH_3)_4$ as a matrix reagent for molecular imprinting in this study. Furthermore, the amine template is expected to behave as a base

catalyst for the hydrolysis−polymerization of $Si(OCH_3)_4$, which can lead to good imprinting around the template molecule.

The proceeding of polymerization was confirmed by ^{29}Si solid-state MAS NMR as shown in Figure 6. To compare the effect of amine on the SiO_2−matrix formation, the stacking of $Si(OCH_3)_4$ was also conducted on an Aerosil 200 support without any attached Rh complexes. Both spectra with three sharp peaks attributed to Q_4, Q_3, and Q_2 Si species reveal that the hydrolysis−polymerization of $Si(OCH_3)_4$ proceeded (Figure 6 (a) and (b)). The 87% amounts of $Si(OCH_3)_4$ employed were hydrolyzed and SiO_2 network formed on the surface. Q_4 bulk species are major for the imprinted sample (Rh_{imp-b}), and Q_2 surface Si species are few compared to that for the reference material without Rh complexes, which indicates that the Rh−amine complex promotes efficiently the hydrolysis−polymerization of $Si(OCH_3)_4$. Q_3 species with an OH group exists sufficiently as shown in Figure 6 (a). The SiO_2 network seems to have a flexible structure with silanol groups, which is quite essential for good imprinting.

The layer-by-layer stacking on the SiO_2 support was demonstrated by NMR measurements in our previous studies.[6,7] After the SiO_2−matrix formation, the Rh_{imp-b} complex (c) in Figure 5 was embedded in the matrix overlayers as proved by Rh 3d XPS in Figure 3, which shows a remarkable decrease in the XPS signals after the stacking. Through the regulation of polymerization temperature, the structure of the Rh−amine complex is maintained after the stacking as characterized by ESR and EXAFS, where there are no significant changes in both spectra (Figure 4 (2) and Table 4).

The removal of the template produces not only a template-shaped cavity but also the formation of an unsaturated active Rh species on the surface. The change in the structure of the attached Rh complexes (Rh_{imp-b}·Rh_{imp-a}) was characterized by the EXAFS analysis. The curve-fitting results of the EXAFS data show a definite change in the structural parameters after the evacuation at 373 K (Table 4). The CN of Rh−N interaction reduced from 4 to 3 approximately, and the *R* of Rh−N shortens from 0.209 (±0.001) nm to 0.205 (±0.001) nm. The decrease in the CN suggests the elimination of one ligand from the Rh_{imp-b} complex as shown in Figure 5. The XPS spectrum for the Rh_{imp-a} sample (D) shows almost no signals (Figure 3), excluding a possibility of the redistribution of the Rh species to the SiO_2−matrix surfaces. The H_2 adsorption experiments reveal that the surface pores over the Rh complexes are preserved in the stacking of SiO_2−matrix overlayers (D in Figure 5). The number of adsorbed H_2 per Rh is about 1 as described above, indicating that almost all the Rh complexes can act as active sites for hydrogenation catalysis. Similar results were also confirmed by the plural stacking of SiO_2−matrix overlayers for the Rh−phosphite complexes, where the diameters of pores capturing the Rh complexes were 0.60−0.67 nm.[6]

Figure 7 shows the energy profile calculated by DFT for the removal of the template ligand that is an important process for the imprinting. There are three possible model structures (b), (c), and (d), which should be considered for the conformation of Rh_{imp-a} with the CN of 3. Structures (c) and (d) are Rh(Amine)(O−Si)(HO−Si) with one amine ligand produced by the elimination of one of the two amine ligands in the Rh_{imp-b}. Structure (b) is $Rh(Amine)_2(O-Si)$ in a unidentate form. An energy barrier of 31 kcal mol^{-1} exists between the initial structure (a) and the structure (c) as shown in Figure 7. This process requires heating at 373 K for 3 h for its completion as characterized by the EXAFS analysis. Further, the energy level of structure (d) produced by the elimination of another amine ligand is 7 kcal mol^{-1} higher than that of structure (c). The difference gives approximately 10^4 times larger rate for the formation of structure (c) from the structure (a) than that for structure (d), assuming a similar difference of activation energy between the two transformations. From the DFT calculation, an amine ligand seems to be eliminated preferentially to form the stable structure (c) and to create a cavity with the template shape behind the amine template. Structure (a) may be in equilibrium with the unidentate structure (b) under the evacuation condition at 373 K, but the energy level of (b) is located 18 kcal mol^{-1} higher than that of (a). Thus the population of structure (b) is negligible under the imprinting condition. The further elimination of the amine ligand in structure (c) is kinetically impossible at 373 K because the whole energy required for the removal of two amine ligands in structure (a) is 74 kcal mol^{-1} as shown in Figure 7. Hence, we conclude that the Rh_{imp-a} complexes on the SiO_2 surface are synthesized step by step by the combination of the attaching technique and the imprinting technique.

Performance of the Rh_{imp-a} Catalyst for Hydrogenation of α-Methylstyrene. Hydrogenation is one of the fundamental reactions in chemical processes, but its shape-selective regulation in particular for alkenes without any functional groups is difficult because of the lack of their chemical interaction with coordination sphere on metal center. In this study, the hydrogenation of α-methylstyrene was conducted on the imprinted Rh complexes to investigate their shape-selective catalytic properties. α-Methylbenzylamine as template has a similar shape to a half-hydrogenated intermediate species in the α-methylstyrene hydrogenation. Thus, α-methylstyrene is expected to enter into the template cavity to be converted to a hydrogenated product through the half-hydrogenated alkyl species without steric hindrance.

$Rh(C_3H_5)_3$, $Rh(C_3H_5)/SiO_2$, Rh_{sup} with two amines, and Rh_{imp-a} with one amine were used as catalysts for the hydrogenation of α-methylstyrene. The reaction rates on the four samples are summarized in Table 5. The homogeneous complex $Rh(\eta^3\text{-}C_3H_5)_3$ has no catalytic activity for the hydrogenation and decomposes rapidly under the reaction conditions. The reaction did not proceed either after the decomposition.

The attached Rh complex, $Rh(C_3H_5)/SiO_2$ also brought about decomposition to form Rh aggregates under the reaction conditions. The initial activity of $Rh(C_3H_5)/SiO_2$ is zero, but the ill-defined decomposed species exhibits somewhat catalytic activity. Similar behaviors are also observed on the Rh_{sup} complex (B) with two amines on SiO_2 as shown in Figure 9, where the decomposition of the attached complex occurs with color change and the catalytic activity is lost eventually. Such metal aggregates loose the property and shape selectivity of intrinsic metal complexes.

On the other hand, the imprinted Rh_{imp-a} complex after the removal of the template amine has a high hydrogenation activity (TOF = 5.2 min^{-1}) under the identical condition (Table 5 and Figure 9). Furthermore, the reaction proceeds linearly, and the Rh structure remains after the reaction, and the Rh_{imp-a} catalyst is durable and reusable. The stability and durability of the coordinatively unsaturated Rh_{imp-a} species are derived from the location of the complex and the wall architecture of the SiO_2−matrix overlayers as shown in Figure 5 (D), which prevent the Rh species form decomposing.

The catalytic activity greatly depends on the evacuation temperature for the elimination of the template as shown in Figure 8. The catalytic activity increases with an increase in the evacuation temperature. The maximum activity is ac-

complished in the temperature range 363−383 K, and the activity decreases due to the dissociation of the amine at higher-temperature treatment, as shown in Figure 8. The increase in the catalytic activity is parallel to the structural change (decrease in the CN of Rh−N) derived from the EXAFS analysis and the DFT modeling. Thus, only the unsaturated Rh_{imp-a} complex after the removal of the template amine is the active species for the catalytic hydrogenation reaction.

Shape-Selective Behavior of the Rh_{imp-a} Catalyst. As amines easily coordinate to an unsaturated Rh complex and the Rh_{sup} complex with two amine ligands has no hydrogenation activity, amines are regarded to act as effective reaction inhibitors for the unsaturated Rh_{imp-a} complex. To investigate the shape-selective behavior of the imprinted Rh site, seven amines with different sizes and shapes were used as inhibitors for the α-methylstyrene hydrogenation. α-Methylstyrene can enter the template cavity and react in the cavity. Therefore, the shape-selective inhibition reflects the size and shape of the cavity.

The smaller benzylamine (Inh. 1) behaves as an inhibitor similar to the template (Inh. 2), which indicates that the template cavity does not affect smaller molecules than the template. This has also been demonstrated in our previous studies on phosphite-imprinted Rh complexes.[6−8] In contrast, significant differences among the larger amine inhibitors were observed (Figure 10). One methyl substitution on the phenyl ring makes it hard to coordinate on the Rh, exhibiting less inhibition (Inh. 3). 1-Methylheptylamine (Inh. 4) is hard to inhibit the reaction, where the amine amount of 1.8 times than that of the template is needed to show the same inhibition (Table 6). Considering that Inh. 4 has the same number of C atoms as the template, this is a shape-selective distinction for molecules. Inh. 5 with a phenyl ring connecting with an ethyl chain also hardly coordinates to the imprinted Rh and hence inhibits the reaction to a less extent (Figure 10 and Table 6). The comparison between benzhydrylamine (Inh. 6) and (1-naphthyl)ethylamine (Inh. 7) reveals the effect of a phenyl ring on the inhibition. A phenyl ring of the naphthyl group is more effective for inhibition than the other phenyl branch of Inh. 6 as shown in Figure 10. These results suggest that the shape and size of the phenyl plane of the inhibitors are much more effective compared to those on the other sp^3 carbon atom.

This study is the first to have succeeded in preparing an amine-imprinted metal complex at a surface. The preceding surface molecular-imprinted metal complexes have been reported with phosphite-imprinted Rh monomer and dimer.

5. Conclusion

A novel molecular-imprinted Rh−amine complex on SiO_2 was designed and prepared by combining two methods of metal-complex attachment and molecular imprinting on the surface. α-Methylbenzylamine was used as a template amine ligand for the surface molecular imprinting. $Rh(C_3H_5)_3$ was attached on a SiO_2 surface, and the amine template coordinated to the attached $Rh(C_3H_5)/SiO_2$ to form $Rh(Amine)_2(OSi)(HOSi)$ species (Rh_{sup}). Molecular imprinting was performed by the stacking of SiO_2−matrix overlayers surrounding the template-coordinated Rh complexes on the surface and the subsequent the removal of the template ligand from the complex embedded in the surface pore. The amine template promoted the hydrolysis−polymerization of $Si(OCH_3)_4$, and a fine SiO_2 network could be constructed around the template. The removal of the template was accomplished by evacuation at 373 K, and an unsaturated Rh conformation with the template-shaped cavity was formed in the surface pore. We characterized all the Rh structures and the surface SiO_2−matrix overlayers by both experimental and theoretical methods. The imprinted Rh complex was highly active for the hydrogenation of α-methylstyrene whose half-hydrogenated alkyl intermediate has a shape similar to that of the template. The $Rh(C_3H_5)_3$ precursor, the attached Rh complex, and the supported Rh−amine complex exhibited no catalytic activity and easily decomposed under the reaction conditions. In contrast, the imprinted Rh_{imp-a} complex shows not only high activity but also durability for the reaction. The SiO_2−matrix overlayers surrounding the unsaturated active Rh_{imp-a} species protect from the gathering of active species. Furthermore, the inhibition of the hydrogenation by seven amine inhibitors demonstrated shape-selective behavior on the imprinted site to discriminate one methyl group and the position of phenyl ring. This study is the first to have succeeded in preparing an amine-imprinted metal complex at a surface. The preceding surface molecular-imprinted metal complexes have been reported with phosphite-imprinted Rh monomer and dimer. We are assured that the strategy will be a promising way to produce novel materials with a higher degree of shape selectivity.

Acknowledgment. This research was performed with the support of the 21st Century COE program by the Ministry of Education, Culture, Sports, Science, and Technology. M.T. also thanks JSPS for the JSPS fellowship. The XAFS measurements were carried out with the approval of the Photon Factory advisory committee (PAC) (Proposal No. 2001G315).

References and Notes

(1) Iwasawa, Y. *Adv. Catal.* **1987**, *35*, 187.
(2) Iwasawa, Y. *Acc. Chem. Res.* **1997**, *30*, 103.
(3) Iwasawa, Y. *Stud. Surf. Sci. Catal. (Proc. 11th Int. Congr. Catal. Baltimore)* **1996**, *101*, 21.
(4) Tada, M.; Iwasawa, Y. *J. Mol. Catal. A: Chemical* **2003**, *199*, 115.
(5) Tada, M.; Iwasawa, Y. *J. Mol. Catal. A: Chemical* **2003**, *204−205*, 27.
(6) Tada, M.; Sasaki, T.; Iwasawa, Y. *Phys. Chem. Chem. Phys.* **2002**, *4*, 4561.
(7) Tada, M.; Sasaki, T.; Shido, T.; Iwasawa, Y. *Phys. Chem. Chem. Phys.* **2002**, *4*, 5899.
(8) Tada, M.; Sasaki, T.; Iwasawa, Y. *J. Catal.* **2002**, *211*, 496.
(9) Suzuki, A.; Tada, M.; Sasaki, T.; Shido, T.; Iwasawa, Y. *J. Mol. Catal. A: Chemical* **2002**, *182*, 125.
(10) Whitcombe, M. J.; Alexander, C.; Vulfson, E. N. *Synlett* **2000**, *6*, 911.
(11) Shellergren, B. *Angew. Chem., Int. Ed.* **2000**, *39*, 1031.
(12) Mosbach, K. *Chem. Rev.* **2000**, *100*, 2495.
(13) Davis, M. E.; Katz, A.; Ahmad, W. R. *Chem. Mater.* **1996**, *8*, 1820.
(14) Wulff, G. *Chem. Rev.* **2002**, *102*, 1.
(15) Strikovsky, A. G.; Kasper, D.; Grun, M.; Green, B. S.; Hradil, J.; Wulff, G. *J. Am. Chem. Soc.* **2000**, *122*, 6295.
(16) Ye, L.; Mosbach, K. *J. Am. Chem. Soc.* **2001**, *123*, 2901.
(17) Hart, B. R.; Rush, D. J.; Shea, K. J. *J. Am. Chem. Soc.* **2000**, *122*, 460.
(18) Yilmaz, E.; Haupt, K.; Mosbach, K. *Angew. Chem., Int. Ed.* **2000**, *39*, 2115.
(19) Brunkan, N. M.; Gagne, M. R. *J. Am. Chem. Soc.* **2000**, *122*, 6217.
(20) Polborn, K.; Severin, K. *Eur. J. Inorg. Chem.* **2000**, 1687.
(21) Cammidge, A. N.; Baines, N. J.; Bellingham, R. K. *Chem. Commun.* **2001**, 2588.
(22) Markowitz, M. A.; Kust, P. R.; Deng, G.; Schoen, P. E.; Dordick, J. S.; Clark, D. S.; Gaber, B. P. *Langmuir* **2000**, *16*, 1759.
(23) Katz, A.; Davis, M. E. *Nature* **2000**, *403*, 286.
(24) Fryzuk, M. D.; Piers, W. E. *Organomet. Synth.* **1986**, *3*, 128.
(25) Stern, E. A.; Newville, M.; Ravel, B.; Yacoby, Y.; Haskel, D. *Phys. B* **1995**, *208*, 117.
(26) Ankudinov, A. L.; Ravel, B.; Rehr, J.; Conradson, S. D. *Phys. Rev. B* **1998**, *58*, 7565.
(27) Delly, B. *J. Chem. Phys.* **1990**, *92*, 508.
(28) Perdew, J. P.; Wang, Y. *Phys. Rev. B* **1992**, *45*, 13244.

(29) Foley, H. C.; DeCanio, S. J.; Tau, K. D.; Chao, K. J.; Onuferko, J. H.; Dybowski, C.; Gates, B. C. *J. Am. Chem. Soc.* **1983**, *105*, 3074.
(30) Ward, M. D.; Harris T. V.; Schwartz, J. *J. Chem. Soc., Chem. Commun.* **1980**, 357.
(31) Ward, M. D.; Schwartz, J. *J. Am. Chem. Soc.* **1981**, *103*, 5253.
(32) Stern, E. A. *Phys. Rev. B* **1993**, *48*, 9825.
(33) Iwasawa, Y.,Ed.; *X-ray adsorption fine structure for catalysts and surfaces*; World Scientific: River Edge, NJ, 1996.
(34) Iwasawa, Y. *Tailored Metal Catalysts*; Reidel: Dordrecht, 1986.
(35) Ward, M. D.; Schwartz, J. *J. Mol. Catal.* **1981**, *11* 397.
(36) Dufour, P.; Houtman, C.; Santini, C. C.; Nedez, C.; Basset, J. M.; Hsu, L. Y.; Shore, S. G. *J. Am. Chem. Soc.* **1992**, *114*, 4248.
(37) Iwasawa, Y.; Sato, H. *Chem. Lett.* **1985**, 507.
(38) Contour, J. P.; Mouvier, G.; Hoogewigs, M.; Leclere, C. *J. Catal.* **1977**, *48*, 217.
(39) Gassman, P. G.; Macomber, D. W.; Willging, S. M. *J. Am. Chem. Soc.* **1985**, *107*, 2380.
(40) Furlani, C.; Mattogno, G.; Plozonetti, G.; Sbrana, G.; Valentini, G. *J. Catal.* **1985**, *94*, 335.
(41) Michalska, Z. M.; Capka, M.; Stoch, J. *J. Mol. Catal.* **1981**, *11*, 323.
(42) Givens, K. E.; Dillard, J. G. *J. Catal.* **1984**, *86*, 108.
(43) Nefedov, V. I.; Firsov, M. N.; Shaplygin, I. S. *J. Electron Spectrosc. Relat. Phenom.* **1982**, *26*, 65.
(44) Nefedov, V. I.; Porai-Koshits, M. A. *Mater. Res. Bull.* **1972**, *7*, 1543.
(45) Nefedov, V. I. *Koord. Khim.* **1978**, *4*, 1285.